Journal of Marine Science and Application (2025) 24: 970-983
https://doi.org/10.1007/s11804-025-00632-5

RESEARCH ARTICLE

Optimizing Geometric Parameters of Planing Vessels for Enhanced Hydrodynamic Performance

Rachid Tayeb[1], Samir E. Belhenniche[1,2], Mustapha Belkadi[1], Mohammed Adnan Rizk[3], Omer Kemal Kinaci[4,5,6] and Pengfei Liu[2]

Received: 25 June 2024 / Accepted: 28 August 2024

Abstract

The hydrodynamic performance of high-speed planing hulls has gained considerable interest, with recent advancements in computational fluid dynamics and hull design techniques enhancing the understanding of planing hull hydrodynamics. In this study, we conducted a numerical investigation using the Reynolds-averaged Navier-Stokes approach with overset grids to capture large motions at high speeds. This study aims to improve the hydrodynamic performances of planing hulls, specifically focusing on total resistance, trim, and sinkage. The initial Fridsma hull with a deadrise angle of 20° has been used for validation, demonstrating good agreement with measurements at different Froude numbers. Subsequently, new configurations based on the Fridsma hull have been designed by varying the deadrise angle, number of chines, and transverse steps. Our findings reveal a correlation between the deadrise angle, the number of chines, and the Froude number. As the deadrise angle increases, total resistance also increases. Additionally, a single chine yields superior results at higher Froude numbers, while multiple chines offer advantages at lower values. The introduction of transverse steps consistently increases total resistance, highlighting their role in improving planing hull performance. This research not only offers valuable insights into planing hull design but also leverages state-of-the-art numerical methods to advance the understanding of hydrodynamic behaviors at high ship speeds.

Keywords Ship resistance; Deadrise angle; Overset grids; Fridsma hull; Planing hull; Single chine; Transverse steps

Article Highlights

- A correlation exists between the deadrise angle, the number of chines, and the Froude number.
- As the deadrise angle increases, total resistance also increases.
- A single chine performs better at higher Froude numbers, while multiple chines are advantageous at lower Froude numbers.
- Introducing transverse steps consistently increases total resistance, highlighting their importance in enhancing planing hull performance.

✉ Rachid Tayeb
rachid.tayeb@univ-usto.dz

[1] Department of Marine Engineering, Aero-Hydrodynamic Naval Laboratory, University of Sciences and Technology USTO-MB, 31000 Oran, Algeria

[2] School of Engineering, Newcastle University, Newcastle Upon Tyne, NE1 7RU, UK

[3] Faculty of Mechanical and Electrical Engineering, Marine Engineering Department, Tishreen University, Lattakia 041, Syria

[4] Faculty of Naval Architecture and Ocean Engineering, Istanbul Technical University, 34460 Istanbul, Turkey

[5] Marine Robotics Laboratory, Istanbul Technical University, 34460 Istanbul, Turkey

[6] Marine Cybernetics Advanced Vehicle Technologies Ltd. (MARNETICS), 34485 ITU ARI Teknokent, Turkey

1 Introduction

The hydrodynamic performance of planing hulls is crucial in ship design and marine engineering, particularly for high-speed crafts. Research in this field aims to reduce resistance and enhance hydrodynamic performance. However, accurately evaluating hydrodynamics at elevated Froude numbers and accounting for complex motions such as trim and sinkage presents considerable challenges. When the Froude number exceeds approximately 1.2, the vessel enters the planing mode (Faltinsen, 2005). During this mode, hydrodynamic forces primarily support the vessel's weight, surpassing buoyancy forces and directly influencing the trim angle.

Numerous investigations, including computation fluid dynamics (CFD) simulations, experimental measurements, and analytical methods, have been extensively employed to analyze the hydrodynamic performance of planing hulls. Savitsky (1964) was the first to successfully formulate and generalize the motions of the hull (trim) and drag (total resistance). His studies continue to be widely used today. Along with his team, Savitsky later identified an additional component of viscous drag in the whisker spray region forward of the stagnation line using an analytical approach

(Savitsky et al., 2007). This viscous drag component, which had not been developed in his earlier studies, aimed to quantify the contribution of the whisker spray to the total planing hull resistance. The study covered a wide range of speeds, deadrise, and trim angles. The analytical and experimental results were in good agreement, showing that the whisker spray drag component accounted for 15% of the total resistance.

In the last decade, Savitsky and Morabito (2010) introduced empirical relations for stepped planing hulls to define longitudinal surface wake profiles. These profiles are influenced by various parameters, such as speed coefficient, deadrise, and trim angles. Considering hydrostatic and hydrodynamic effects along with the deadrise angle, trim, and wetted length, Morabito (2014) later developed empirical equations to estimate the pressure distribution at the bottom of planing hulls. The study revealed the applicability of these equations across a wide range of deadrise angles (0° to 40°), trim angles (up to 30°), and wetted length-to-beam ratios (up to 5.5).

In the last decade, numerous numerical studies have explored the hydrodynamics of planing hulls. Yousefi et al. (2014) conducted numerical simulations of a high-speed planing hull with two tunnels on the bottom section to reduce drag. They used the $k–\varepsilon$ turbulence model and applied the VOF method to capture free-surface deformations around the hull. The study found that the tunnels notably reduced resistance, with up to 14% reduction at a forward speed of 60 knots. Mousaviraad et al. (2015) investigated the motions, accelerations, and slamming characteristics of high-speed planing hulls using the CFD Ship-Iowa code, employing single-and two-phase volume-of-fluid (VOF) solvers. Simulations were conducted in calm water and waves for deep and shallow conditions. The results for trim, sinkage, total resistance, and seakeeping performance in regular and irregular waves showed good agreement with experimental data.

Sukas et al. (2017) later conducted numerical simulations of the Fridsma hull using the commercial software STAR-CCM+ with overset grids. They resolved the two-phase flow using the VOF method and activated the dynamic fluid-body interaction (DFBI) model. Their study divided the resistance components and illustrated trim and sinkage using a rigid body approach to effectively understand planing hull hydrodynamics. The findings revealed that the overset grid system yielded results closely matching experimental data at high Froude numbers, while the rigid body approach was more accurate at low Froude numbers. Kahramanoğlu et al. (2020) demonstrated that a two-degree-of-freedom model is sufficient to predict heave and pitch motions for monohedral and warped hulls using overset grids. Their study showed that the Reynolds-averaged Navier-Stokes (RANS) method provides highly accurate predictions of the vertical motions of planing hulls.

Several semi-empirical methods for calculating the resistance of planing hulls have also been proposed. Wang et al. (2023) introduced a new semi-empirical method, the M-S method, derived from equations presented by Morabito (2014) to determine resistance, trim, sinkage, and pressure distribution on the planing hull bottom. Numerical results showed good agreement with the Savitsky method, the M-S method, and experimental data. Research on high-speed planing hulls has also extended to catamarans. Wang et al. (2022) conducted experiments and numerical simulations for a high-speed planing catamaran in calm water under different displacements. They employed overset grids to simulate large motions. Using two different turbulence models, $k–\omega$ shear stress transport (SST) and realizable $k–\varepsilon$, the obtained sinkage and trim angles agreed well with the experiments, with the $k–\omega$ SST model providing slightly more accurate results for total resistance.

In addition to the aforementioned numerical studies, several towing tank test results have been conducted and published in the literature to evaluate the hydrodynamic performance of planing craft. Recent studies include the work by Taunton et al. (2010), who performed a series of experimental tests to investigate the influence of stepped hulls on the hydrodynamic performance of high-speed crafts with a constant deadrise of $\beta = 22.5°$ in calm water and waves. The tests showed that adding transverse steps notably reduced resistance by decreasing the wetted area, with single and double steps decreasing resistance by 26.5% and 25.4%, respectively. Begovic and Bertorello (2012) conducted experimental studies on three warped and one monohedral hull model, varying deadrise angles along the hull length to evaluate hydrodynamic performance. The results indicated that monohedral hulls exhibit less resistance than warped hulls. De Luca and Pensa (2017) investigated the influence of the length-to-displacement ratio and the effectiveness of interceptors on five hard chine models, with and without interceptors, in planing and semi-planing speed ranges. The study revealed that hulls equipped with interceptors showed a decrease in trim angle and a substantial reduction in lift-induced resistance.

Vitiello et al. (2022) experimentally investigated a series of stepped hulls with various configurations, focusing on step height and longitudinal center of gravity (LCG) position. The hulls featured a transparent bottom to observe the wetted surface area and the development of vortices generated behind the steps. The study found that changes in the LCG affected resistance, and increasing step height led to a reduction in resistance. A recent study by Lakatos et al. (2022) presented experimental results on the impact of various design parameters, including spray rails, chine strips, and V-shaped spray interceptors (VSIs), on the performance of planing hulls in calm water. The results indicated that spray rails reduced resistance by up to 2.4%. Additionally, chine strips contributed to a reduction in trim by 0.3° and total resistance by up to 3%. The study also showed that

placing the VSI forward of the stagnation line decreased total resistance by 4.2%, whereas positioning it behind the stagnation line increased total resistance by 8.4%.

The present research aims to conduct numerical investigations using various planing hull configurations based on the Fridsma planing hull. These investigations involve varying the deadrise angle, number of chines, and transverse steps to assess their effects on planing hull hydrodynamics. The analysis focuses on ship resistance, sinkage, and trim angle. Based on RANS equations, the commercial numerical code STAR-CCM+ was used. Following the introduction, Section 2 defines the planing surface geometry and introduces the model used in the study. Section 3 outlines the mathematical approach and details the integration of numerical algorithms into the model. Section 4 presents the results based on the simulations, including a validation case. Section 5 concludes the study by summarizing the contributions.

2 Geometric properties of the planing vessel

In the planing regime, a boat moves through the water at high speed, generating waves and resulting in the formation of two distinct spray patterns:

- Whisker spray, which originates at the spray root line.
- Main spray, which appears where the spray root line intersects with the chine.

The geometric details of a planing vessel are partially influenced by its generated waves. Figure 1 illustrates a high-speed planing hull, summarizing key geometric parameters such as beam B, trim angle τ, and deadrise angle β. The wetted lengths of the keel L_K and chine L_C are also depicted and expressed as follows:

$$L_K = \frac{B \tan \beta}{2 \tan \tau} \tag{1}$$

$$L_K - L_C = \frac{B \tan \beta}{\pi \tan \tau} \tag{2}$$

The main wetted length-to-beam ratio λ is

$$\lambda = \frac{0.5(L_K + L_C)}{B} \tag{3}$$

The planing hull geometry used in this study is the Fridsma hull, named after Gerard Fridsma, who developed the series in the 1960s to conduct a systematic study aimed at understanding the performance of planing boats (Fridsma, 1969). Fridsma hulls remain widely used as benchmark ships for numerical and experimental studies. These hulls have a prismatic shape based on analytical expressions and feature a single chine line, as demonstrated in Figure 2. The model maintains a deadrise angle of 20° from bow to stern with a ratio L/B = 5. The LCG is located at 60% L from the bow, and the displacement coefficient is C_Δ = 0.608. Table 1 presents the details of Fridsma hull geometry used in this study.

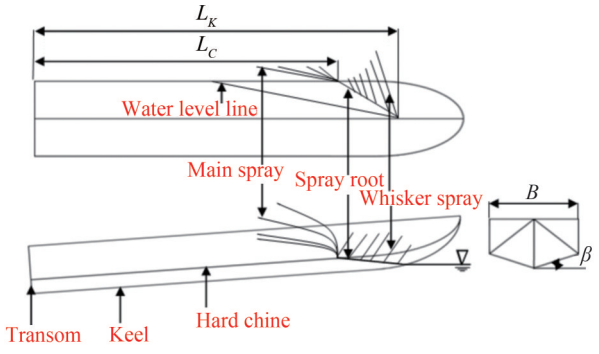

Figure 1 Geometric details of planing vessels

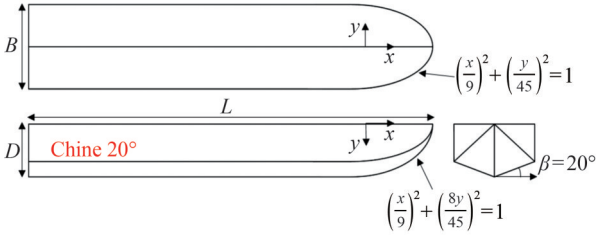

Figure 2 Mathematical expressions to form the lines of Fridsma hulls

Table 1 Main dimensions of the Fridsma hull used in this study

Parameter	Symbol	Value
Length overall (m)	L	1.143
Beam (m)	B	0.228
Draft (m)	T	0.051
Dept (m)	D	0.114
Deadrise angle (°)	β	20
Longitudinal center of gravity (m)	LCG	0.457
Vertical center of gravity (m)	VCG	0.067
Displacement weight (kg)	Δ	7.260
Moment of inertia (kg·m^2)	$I_{YY} = I_{ZZ}$	0.592

3 Mathematical approach and numerical implementation

This section is dedicated to the mathematical approaches used in this study and the numerical implementation of the CFD approach. We first explain the empirical relations of Savitsky. Then, the mathematical background, numerical algorithms, and the implemented grid methodology are presented.

3.1 Savitsky's empirical approach

Savitsky proposed a semi-empirical approach in 1964 to understand and model planing crafts. This method relies on multiple experimental trials to evaluate hydrodynamic and hydrostatic performances, including pressure and viscous resistance, wetted length, and trim angle. This section offers a comprehensive overview of the Savitsky method, encompassing all crucial details. The Froude number based on the beam is defined as follows:

$$Fr_B = C_V = \frac{V}{\sqrt{gB}} \tag{4}$$

The lift coefficient of the planing hull is defined as follows:

$$C_{L\beta} = \frac{\Delta}{0.5\rho V^2 B^2} \tag{5}$$

$$C_{L\beta} = C_{L0} - 0.006\,5\beta C_{L0}^{0.6} \tag{6}$$

where the lift coefficient for a flat plate is $\beta = 0$. Herein, C_{L0} is given as

$$C_{L0} = \tau^{1.1}\left(0.012\sqrt{\lambda} + \frac{0.005\,5\lambda^{\frac{5}{2}}}{C_V^2}\right) \tag{7}$$

We consider the equilibrium condition l_P = LCG. The mean wetted length-to-beam ratio λ is calculated as follows:

$$\frac{l_P}{\lambda b} = 0.75 - \frac{1}{5.21\frac{C_V^2}{\lambda^2} + 2.39} \tag{8}$$

where l_P is the center of the hydrodynamic pressure measured along the keel from the transom stern.

$$R_n = \frac{VL}{\nu} \tag{9}$$

$$C_F = \frac{0.075}{\left(\log_{10}R_n - 2\right)^2} \tag{10}$$

where C_F is the frictional resistance coefficient according to the ITTC57 correlation line. Pressure and viscous resistances are respectively expressed by the following equations:

$$R_P = \Delta\tan\tau \tag{11}$$

$$R_F = \frac{\rho V^2 C_F \lambda B^2}{2\cos\beta\cos\tau} \tag{12}$$

In this case, the total resistance is the summation of the two resistance components:

$$R_T = R_P + R_F \tag{13}$$

Equation (13) returns the total resistance of a planing hull. However, Savitsky's empirical relations are notably used between the following ranges: $0.6 < C_V < 13$, $2 < \tau < 15$, and $\lambda \leqslant 4$.

3.2 Computational approach

Numerical investigations were conducted using the commercial code STAR-CCM+, which is based on the finite volume method for solving the conservation of mass and momentum equations in unsteady flow. In this study, the physical domain was discretized using the VOF approach, which is suitable for capturing the free surface in multiple flow fluids. The $k-\varepsilon$ turbulence model (Menter et al., 2003) was employed to model turbulent flow, and the DFBI model was activated to account for the free motions of heave and pitch. A semi-implicit pressure-linked equation algorithm was used for pressure–velocity coupling. The convection and diffusion terms were discretized using a second-order upwind. The governing equations are stated as follows:

$$\frac{\partial\rho}{\partial t} + \frac{\partial\left(\rho u_i\right)}{\partial x_i} = 0 \tag{14}$$

$$\frac{\partial\left(\rho u_i\right)}{\partial t} + \frac{\partial\left(\rho u_i u_j\right)}{\partial x_j} = -\frac{\partial p}{\partial x} + \frac{\partial}{\partial x_j}\left(\mu\frac{\partial u_i}{\partial x_j} - \overline{\rho u_i' u_j'}\right) \tag{15}$$

Based on the recommendation of ITTC CFD (ITTC 7.5-03-02-03, 2011), the time step used is a function of the planing hull's speed and length. The time step, calculated using the equation expressed below, was selected for all cases, with 10 inner iterations performed per time step.

$$\Delta t = \left[0.005, 0.01\right]\frac{L}{V} \tag{16}$$

The computational domain used is divided into two parts: the background and the overset parts, as shown in Figure 3. According to CFD guidelines of the ITTC (ITTC 7.5-03-02-03, 2011), the inlet, side wall, top, and bottom boundaries are located at 4 L, 4 L, L, and 4 L respectively, from the planing hull, and are all defined as velocity inlets. The outlet, located at 8 L behind the planing hull, is set as a pressure outlet. For the overset region, the hull surface is defined with a no-slip condition, and the interfaces between the two parts are assigned as overset conditions. A symmetry condition was imposed by using a half domain to reduce the computational time.

The planing motion within the fluid domain was modeled using overset grids, a technique that involves dividing the computational domain into overlapping cells. One of the advantages of this mesh implementation lies in its capability to eliminate the need for modification post-generation.

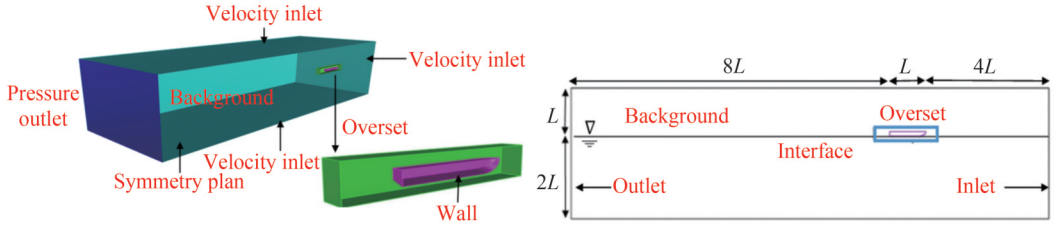

Figure 3 Details of the computational domain and the associated boundary conditions

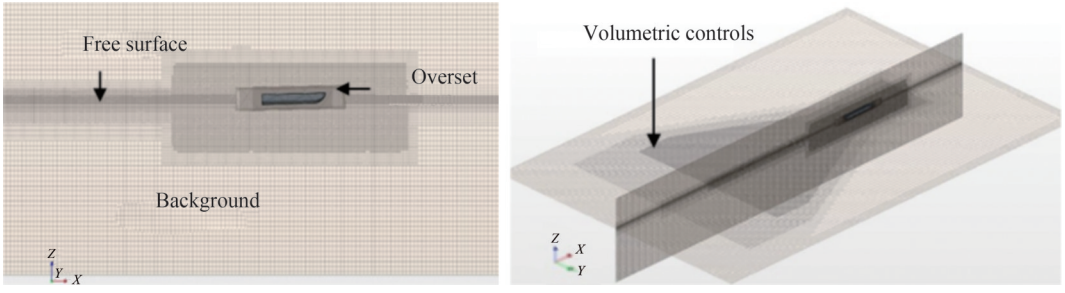

Figure 4 Grid topology from different views

Anisotropic mesh refinement was used for the uncertainty mesh study, which involved preparing coarse, medium, and fine meshes with hexahedral-shaped cells. The cell number was multiplied by a grid refinement ratio $r_G = \sqrt{2}$ to enhance the accuracy of the results (Stern et al., 2001). Six volumetric controls were established to capture Kelvin waves and the free surface. Figure 4 presents various views of the mesh topology used.

For accurate results, eight prismatic layers were generated adjacent to the planing hull wall, with the height of the first cell (y) fixed at 0.003 5 m. Figure 5 illustrates the distribution of y^+ on the Fridsma hull. This study was conducted on the Fridsma hull with a deadrise angle of 20° at Fr = 0.9. The number of cells for coarse, medium, and fine meshes was around 1.6 M, 2.25 M, and 3.2 M, respectively.

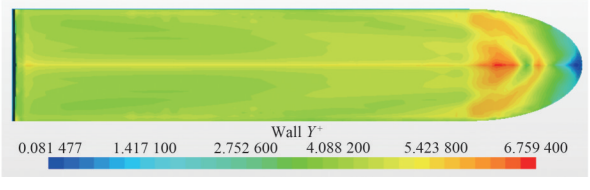

Figure 5 Visualization of y^+ for the original Fridsma hull at Fr = 0.9

4 Results

In this section, we first present the hydrodynamic performance results of the original Fridsma planing hull and compare them with the experiments and the Savitsky method. The findings for the new configurations, designed based on the parametric study, are thoroughly examined to elucidate their behavior across a broad range of Froude numbers, covering displacement, transition, and planing modes. These results offer a comprehensive assessment of the numerical performance and fundamental physics governing planing vessels and their behavior in the planing regime.

4.1 Validation

Numerical simulations were performed for the Fridsma hull with a deadrise angle β = 20°, a length-to-beam ratio L/B = 5, and a displacement coefficient C_Δ = 0.608 using different grids. The obtained results were compared with those from the Savitsky method (Savitsky, 1964) and the experimental data provided by (Fridsma, 1969). Figure 6 illustrates the rotation and translation of the overset region and its cells during the initialization of the solution and after computation. The figure also reveals the initial position of the vessel before computations began and the steady-state condition of the vessel achieved at the end of the simulation.

As shown in Table 2, the obtained results for resistance, trim, and sinkage depend on the grid. The total resistance and sinkage are nondimensionalized with displacement force and beam, respectively. Some differences are observed between the different grids, with considerable differences in trim values, even with the fine grid. However, the relative error with the fine grid is remarkably low and closely matches the experimental results. Therefore, the parametric study in this research is conducted using the fine grid. Table 2 provides the number of cells in the grids.

The convergence of the numerical results is demonstrated by the time history graphs of resistance, trim, and sinkage plotted in Figure 7(a) for Fr = 0.9. Convergence was achieved after 7 s of real-time simulation. Figure 7(b) presents a comparison of the simulation results with those from the Savitsky method and experimental data across a Froude number

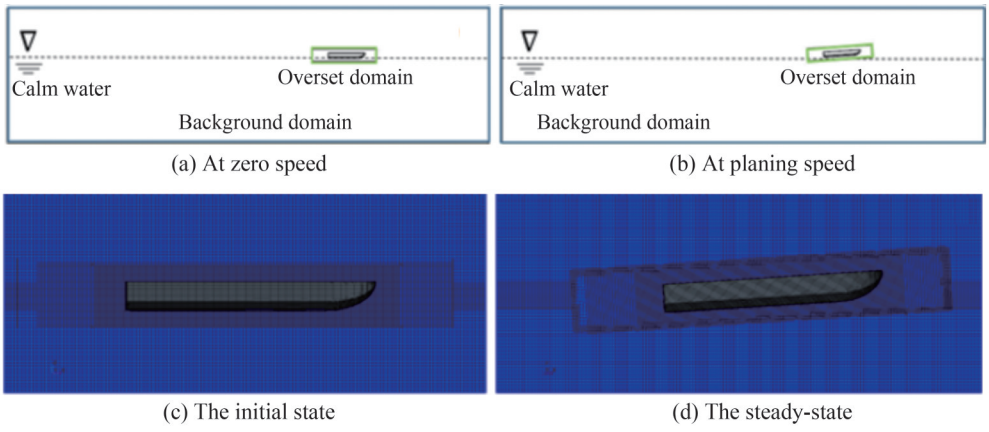

Figure 6 Description of the overset mesh method implemented in numerical simulations and the appearance of the grid

Table 2 Resistance, trim, and sinkage of the Fridsma hull compared with experiments at $Fr = 0.9$

Grid	No. of cells	R_T/Δ			$\tau(^\circ)$			sk/B		
		CFD	EFD	Err (%)	CFD	EFD	Err (%)	CFD	EFD	Err (%)
Coarse	1.6 M	0.133 4		4.17	3.339 5		8.76	0.013 4		14.18
Medium	2.2 M	0.130 0	0.128 0	1.50	3.101 8	3.666 0	15.25	0.014 8	0.015 0	4.95
Fine	3.2 M	0.127 9		0.08	3.293 1		10.00	0.015 5		0.84

range of $0 \leqslant Fr \leqslant 1.5$ for total vessel resistance. The numerical simulations in this study align well with the experimental data during the displacement and transition phases. However, some differences are observed in the planing regime. Regarding trim, as shown in Figure 7(c), the computational results are consistent with those of Savitsky, but a remarkable difference is noted in the planing regime compared to the experimental results. Sinkage values, displayed in Figure 7(d), are in perfect agreement with the experimental values across the entire speed range.

4.2 Effect of deadrise

In this section, we investigate the impact of deadrise angle on the hydrodynamic performance of the planing hull was investigated. Three configurations were tested: Fridsma hull with different deadrise angles of 10°, 20°, and 30°. Figure 8 illustrates the configurations of Conf. A ($\beta = 10°$), Conf. B ($\beta = 30°$), and the Fridsma hull, which is characterized by a deadrise angle of $\beta = 20°$. Numerical investigations were conducted for all the same load coefficient $C_\Delta = 0.608$.

The effect of deadrise becomes more pronounced with increased speed. Figure 9(a) shows the calculated results for total resistance across a wide range of Froude numbers. At low Froude numbers, the obtained results are slightly close for different configurations. However, in the planing regime, resistance increases with the deadrise angle. For Froude numbers $Fr \geqslant 0.9$ the reduction in the total resistance for Conf. A is estimated to be approximately 25%. Conversely, Conf. B exhibits higher resistance compared to the initial Fridsma hull. This difference is evident in the wetted area contours, characterized by the volume fraction of water shown in Figure 9(b). In this figure, the vessel is in the planing regime, where 0 and 1 denote air and water, respectively. The figure indicates that Conf A. nearly completely clears itself from water, whereas Conf. B interferes more with water. As a result, Figure 10 shows that high deadrise angles lead to high wave generations. The presence of main and whisker sprays near the hard chine appears to be the underlying reason for the remarkable increase in total resistance in the planing regime. However, small deadrise angles reduce the spray pattern.

The deadrise angle does not affect total resistance in the displacement regime; however, deviations begin once the vessel enters the transition phase. The differences become more pronounced in the planing regime, where lower deadrise angles result in lower resistance. This phenomenon is important because the decrease in resistance occurs despite an increase in the ship's draft (the draft increases because the load coefficients remain the same). The authors question whether this reduction in resistance is valid even for negative-deadrise angles. Matveev and Morabito (2020) investigated such a case and noted that a negative deadrise can result in higher lift capabilities. Although the highest lift-drag ratio is achieved at zero deadrise, they state that eliminating side wetted areas on negative-deadrise hulls may notably enhance hydrodynamic efficiency. Conf. A in Figure 10 supports this statement, as the spray is notably reduced with a lower deadrise, leading to a substantial reduction in resistance.

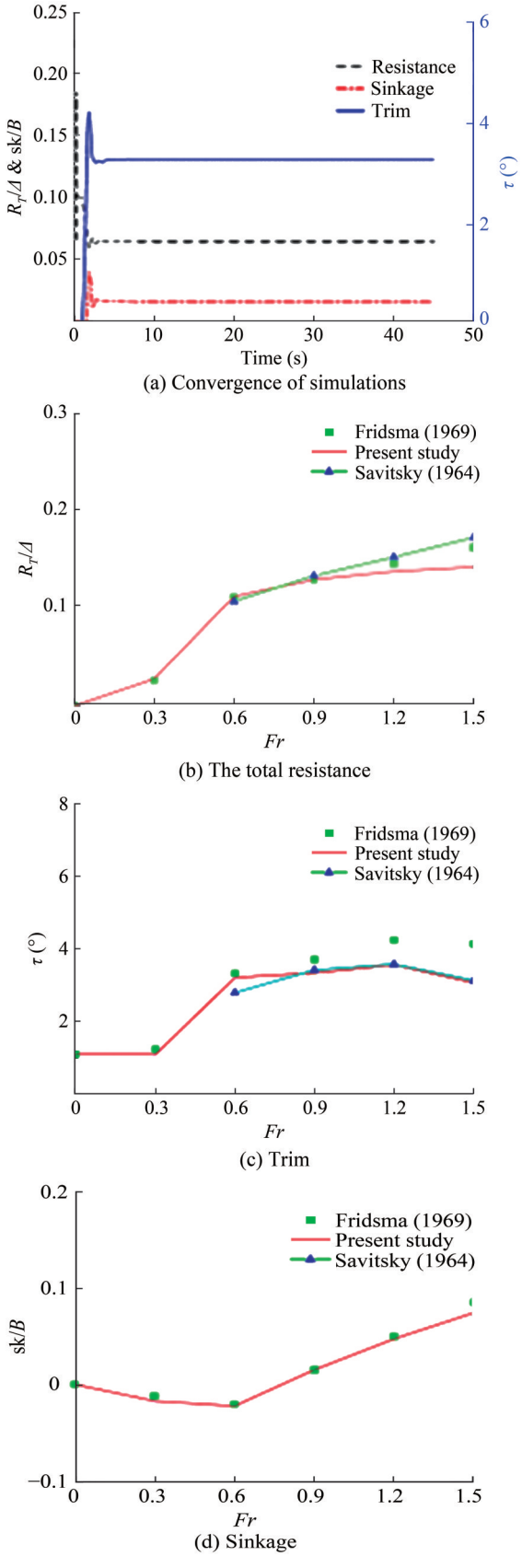

Figure 7 Time histories and comparison of the performance for different Froude numbers

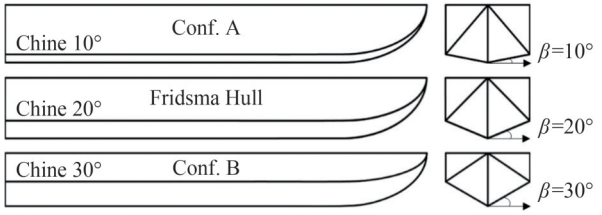

Figure 8 Illustration of variation in deadrise angles of the planing vessels

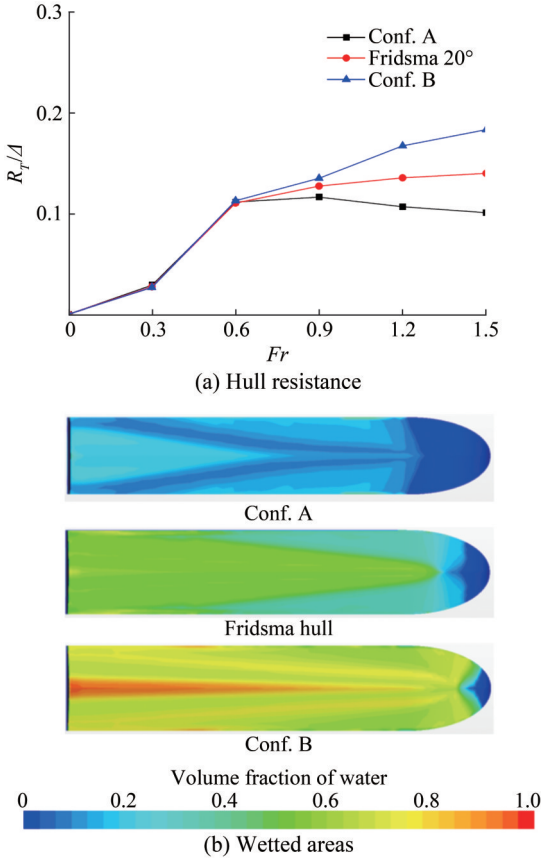

Figure 9 Effect of deadrise angle on hull resistance and wetted areas viewed from the bottom of the hull

The variation in trim angle is plotted in Figure 11(a). Herein, in the displacement phase, the deviations are negligible, but differences become evident once the planing regime is reached. Conf. A, with its low deadrise angle, exhibits a higher trim compared to the other configurations. However, no generalized statement can be made due to the Fridsma Hull, which has a deadrise angle of β = 20°, has a lower trim than Conf. B (β = 30°) at Fr = 1.5. The sinkage curves relative to vessel speed are given in Figure 11(b). At low Froude numbers, $Fr \leqslant 0.6$, sinkage decreases and reaches its minimal values at Fr = 0.6. This decrease is attributed to the negative pressure region below the vessel, as detailed in (Sukas et al., 2017). However, sinkage starts to increase when $Fr > 0.6$, with the hull rising above the water due to remarkable hydrodynamic lift forces.

Based on this figure, Conf. B reduces sinkage by 8% compared to the initial Fridsma hull. The detailed quantitative values of total resistance, trim angle, and sinkage values obtained by varying the deadrise angle and the ship speed are listed in Table 3.

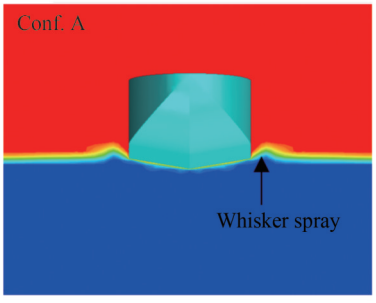

(a) Conf. A - $\beta = 10°$

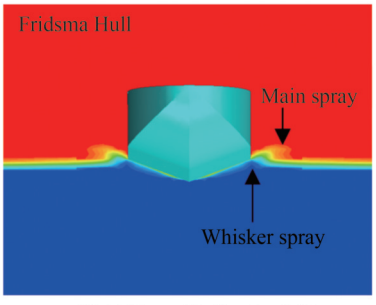

(b) Fridsma Hull - $\beta = 20°$

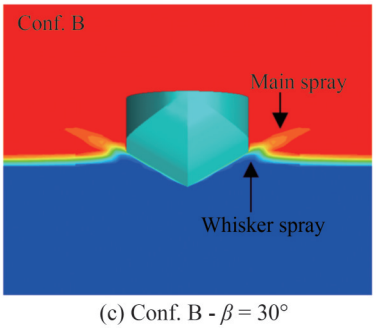

(c) Conf. B - $\beta = 30°$

Figure 10 Spray of the free surface for calm water at $Fr = 1.5$

Figure 12 illustrates the wave elevations along the hull (where viscous effects are dominant) and the wake at $Y/L = 0.2$ for $Fr = 0.9$ and $Fr = 1.5$. As shown in the figure, the deadrise angle substantially impacts wave elevation. As the Froude number increases, wave elevations become highly pronounced in the bow and wake regions. In the planing regime, wave elevations are notably smaller with lower deadrise angles, with the lowest elevations on the free surface achieved by Conf. A.

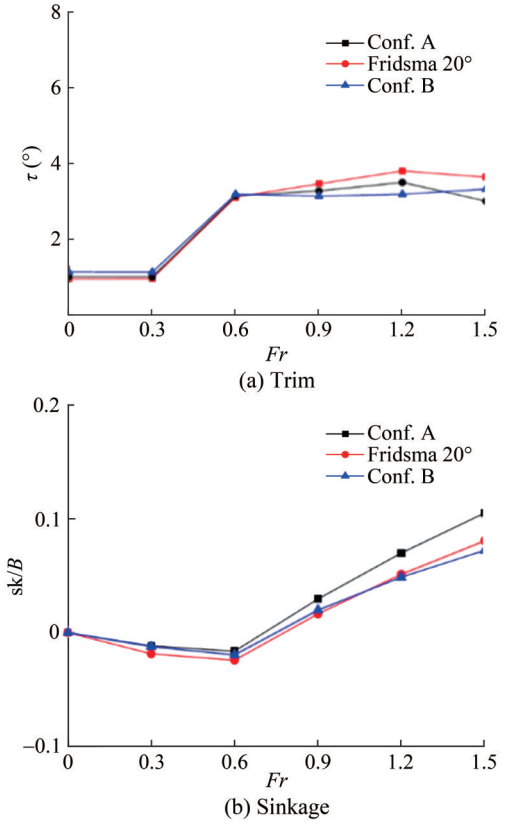

Figure 11 Effect of deadrise angle

4.3 Effect of chines

In this section, numerical simulations were conducted to examine the effect of chine steps on planing hull performance. New configurations derived from the original Fridsma hull were designed by varying the number of chines, as shown in Figure 13. The initial deadrise angle of the original Fridsma hull is maintained in the new geometries. Table 4 provides the details of the newly created geometries.

The effect of chines on total resistance at different ship speeds is shown in Figure 14(a). Similar to the deadrise angle, the chines do not substantially affect resistance in the displacement regime. However, as speed increases, the presence of chines reduces resistance. Despite exhibiting highly nonlinear behavior with the number of chines on

Table 3 Resistance, trim, and sinkage (sk) for different deadrise angles and vessel speeds

Configuration	β	$Fr = 0.3$			$Fr = 1.5$		
		R_T/Δ	$\tau(°)$	sk/B	R_T/Δ	$\tau(°)$	sk/B
Conf. A	10	0.029 1	0.974 3	−0.011 0	0.101 4	3.659 2	0.099 7
Fridsma	20	0.027 4	1.018 5	−0.011 8	0.140 7	3.047 6	0.076 4
Conf. B	30	0.026 7	1.146 1	−0.011 6	0.184 3	3.340 9	0.068 5

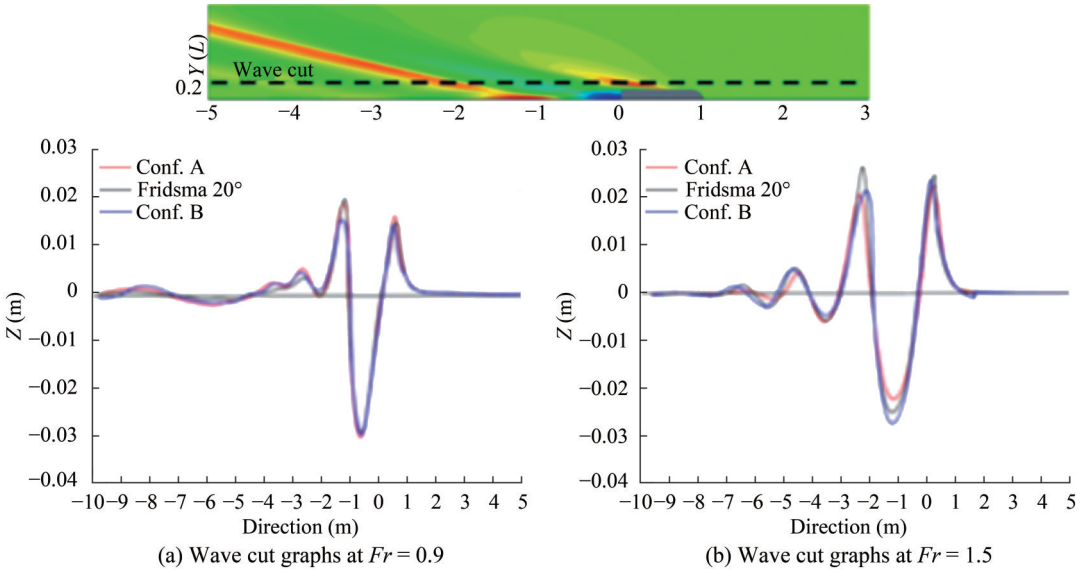

Figure 12 Free-surface deformations and the position of the wave cut

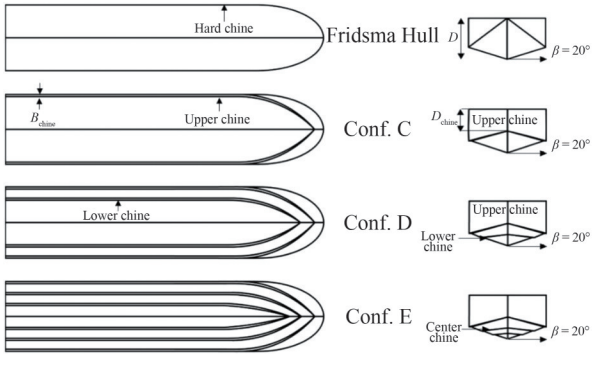

Figure 13 Different chine configurations of planing hull

the vessel, all configurations (Conf. C, Conf. D., and Conf. E) demonstrated lower resistance compared to the initial Fridsma hull form.

Table 4 Geometric properties of new chine configurations

Configuration	Type	B_{Chine}	D_{Chine}
Fridsma	Hard chine	-	-
Conf. C	One chine		4*D*/8
Conf. D	Double chine	*B*/20	7*D*/8
Conf. E	Triple chine		6*D*/8

As demonstrated in Figures 14(b) and 14(c), the Chines reduce trim and elevate the vessel across nearly the entire speed range. Therefore, the chines help position the vessel better to align with flow characteristics. To understand this condition, we visualized the main and whisker sprays at the free surface, as illustrated in Figure 15. Comparing the resistance results at Fr = 1.5, Conf. C reduced total resistance by 12%. This reduction is evident in this figure, which shows the disappearance of spray in Conf. C.

We then divided the total resistance into its pressure and frictional components, with results presented in Figure 16(a) and Figure 16(b), respectively. We examined these resistance components to investigate the reason for the resistance reduction with the introduction of chines and noticed that the difference arises from the sinkage of the vessel. The results displayed in Figure 14(b) indicate that at low speeds, the trim angle of the configurations is slightly lower than that of the Fridsma hull. However, as the Froude number increases, particularly after $Fr > 0.9$, the trim angle becomes more notable. This result is primarily due to the center of pressure shifting aftward, which lifts the bow. Consequently, configuration hulls with chines move higher above water, as illustrated in Figure 14(b). The initial Fridsma hull cannot rise above the water level as effectively as the other configurations in the planing regime of the vessel. Despite having similar pressure resistances, the frictional resistance is notably higher at Fr = 1.5. This phenomenon leads to a greater wetted area of the vessel, which generates higher frictional resistance, as illustrated in Figure 16(b).

At low speeds, the pressure resistance component of the configurations is lower than that of the Fridsma hull, indicating no notable effect on pressure resistance in the planing mode. However, the frictional resistance component of all configurations is slightly higher in the displacement regime, counteracting the dominance of pressure resistance on the total resistance. Table 5 presents the numerical values for resistance, trim angle, and sinkage in the displacement and planing modes of the vessel.

In combination with trim and sinkage dynamics, the inclusion of chine results in reduced total resistance. This reduction also affects the wave generated by the planing vessel, as depicted in Figure 17(a), which displays the free-

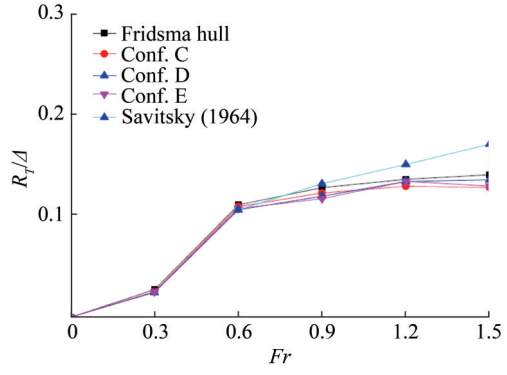

(a) Total ship resistance

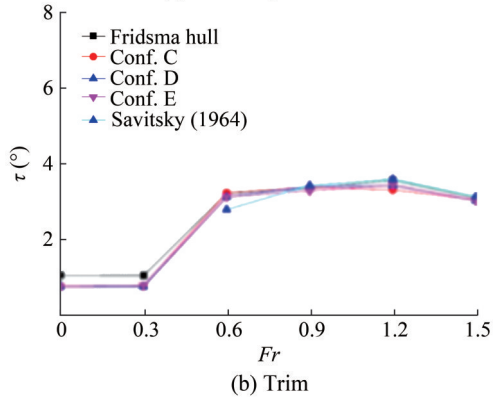

(b) Trim

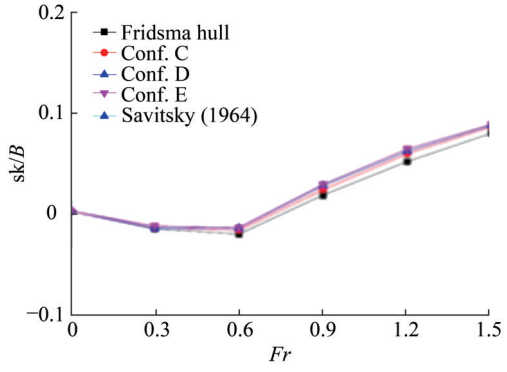

(c) Sinkage

Figure 14 Comparison of the performance for different chine configurations

surface deformations at $Fr = 1.5$. The free-surface contours exhibit compatibility; therefore, we plotted the wave cuts at $y/L = 0.2$, as shown in Figure 17(b). While wave elevations along the vessel are similar, they are remarkably different in the wake regions. All configurations exhibited lower wave elevations in the wake region, which partially explains the reduction in resistance compared to the original Fridsma Hull. The differences in flow patterns and ship dynamics due to different chine configurations collectively influence wave formation in the planing mode.

4.4 Effect of transverse steps

In this section, numerical investigations were conducted

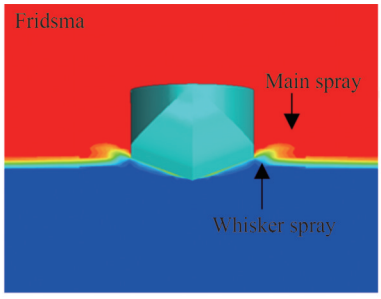

(a) Fridsma hull

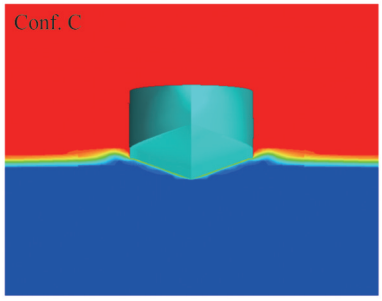

(b) Conf. C

Figure 15 Free-surface deformations at the mid-cross section

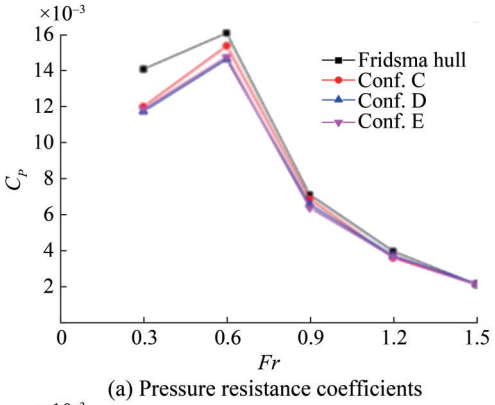

(a) Pressure resistance coefficients

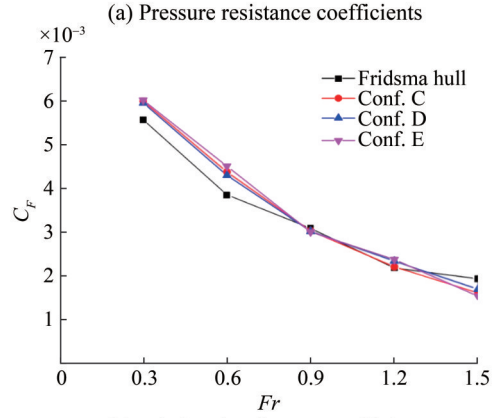

(b) Frictional resistance coefficients

Figure 16 Resistance component

to examine the effect of transverse steps on the hydrodynamic performance of the planing hull. New configurations were tested by varying the number of transverse steps based on the original Fridsma hull form, as illustrated in Figure 18. All configurations maintain a similar dead-

Table 5 Resistance, trim, and sinkage for different chine configurations and vessel speeds

Configuration	Fr = 0.3			Fr = 1.5		
	R_T/Δ	τ(°)	sk/B	R_T/Δ	τ(°)	sk/B
Fridsma	0.027 4	1.018 5	−0.011 8	0.140 7	3.047 0	0.076 4
Conf. C	0.025 2	0.733 0	−0.018 6	0.124 4	2.731 9	0.103 7
Conf. D	0.024 4	0.724 5	−0.016 6	0.135 7	2.291 1	0.084 6
Conf. E	0.024 8	0.752 8	−0.014 4	0.129 5	2.975 1	0.085 5

rise angle (β = 20°) and one hard chine, consistent with the original vessel form. The frontmost step is located at 0.3 L from the aft in all configurations. The second step is at 0.2 L from the aft in Conf. G and Conf. H, while the third step, which is only available in Conf. H, is positioned at 0.15 L from the aft. The height of all transverse steps is 4.1 mm, which corresponds to only 0.36% L of the planing vessel.

In terms of ship speed, various vessels displayed different trends in total resistance, as depicted in Figure 19(a). However, none of them achieved lower resistance than the original Fridsma hull. The original hull design showed a gradual increase in resistance at higher Froude numbers, with minimal changes in the transition and planing phases. In contrast, the new configurations exhibited a linear increase in resistance, even when transitioning into the planing mode. This increase is attributed to the additional transverse steps, which caused the vessel to tilt backward, resulting in unnecessary trim. The changes in trim are illustrated in Figure 19(b). Consequently, the underwater hull shape became bluffer and less aligned with the flow. Compared to the configurations, the superior flow alignment of the Fridsma hull also allowed the vessel to rise higher above the waterline, substantially reducing its total resistance. Sinkage values for all configurations are given in Figure 19(c). The original Fridsma hull maintained a higher position above the waterline across the entire ship speed range.

The bluffer underwater body forms of all configurations lead to higher pressure resistance, as depicted in Figure 20(a). A higher number of steps leads to higher pressure resistance coefficients. By contrast, the frictional resistance coefficient is slightly higher for the initial Fridsma hull, as shown in Figure 20(b). Despite rising higher above the water, the total wetted area of the original hull is greater, leading to higher frictional resistance.

The pitch and heave motions (trim and sinkage, respec-

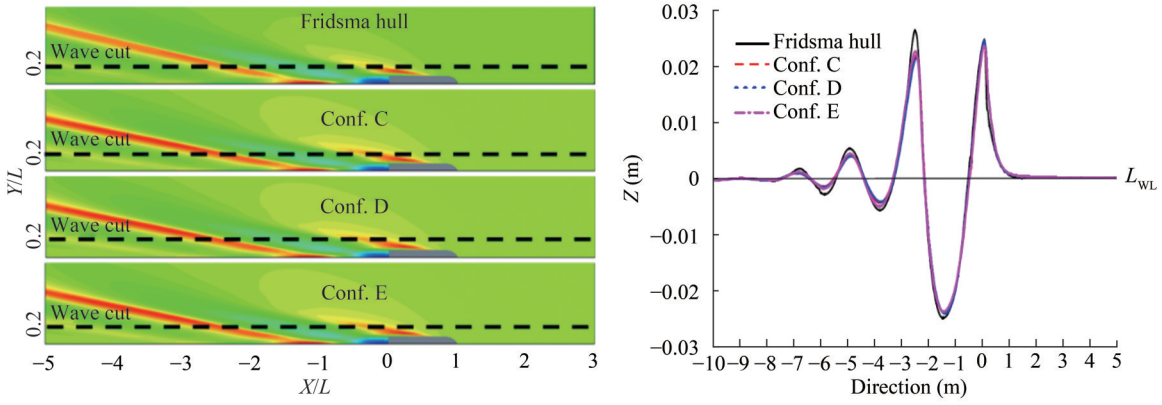

(a) Free-surface deformations (b) Wave cuts

Figure 17 Free-surface deformations and the positions of wave cut for all configurations at Fr = 1.5

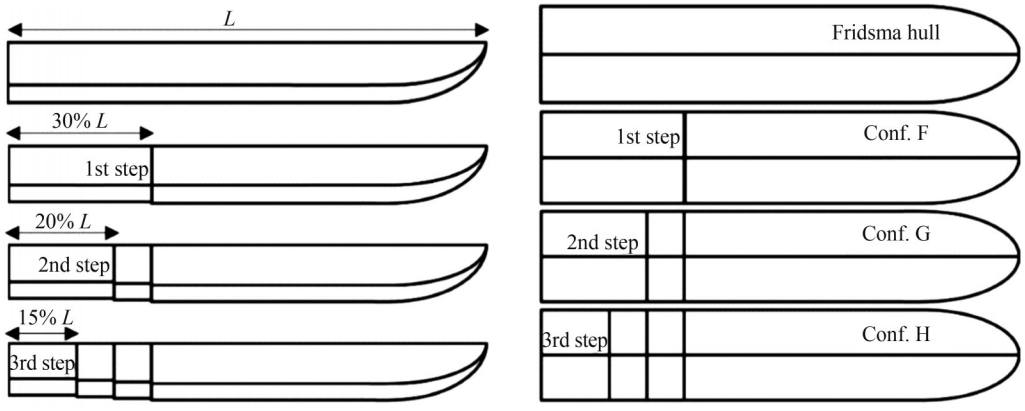

Figure 18 Different transverse step configurations of the planing hull

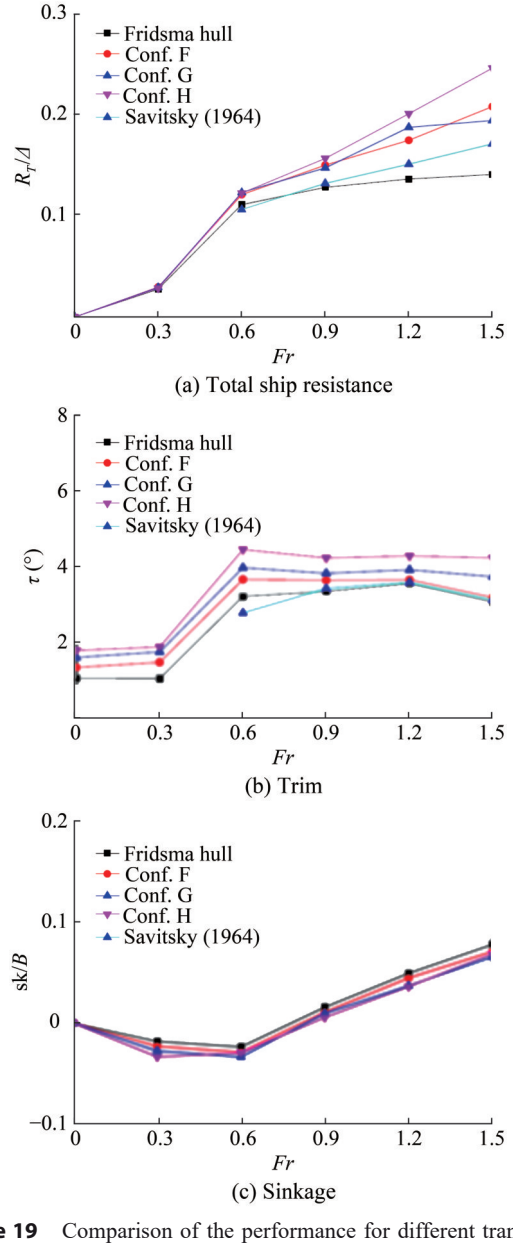

Figure 19 Comparison of the performance for different transverse step configurations

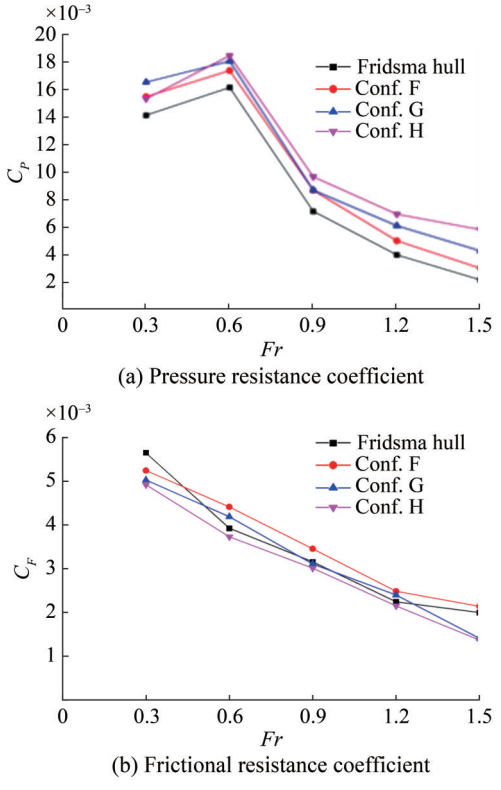

Figure 20 Effect of transverse steps on the resistance component

tively, in the current study) have also been examined by various researchers. Esfandiari et al. (2020) noted that the amplitudes of heave for stepped hulls decrease compared to non-stepped hulls. We observed a similar pattern to heave, as shown in Figure 19(c), indicating reduced sinkage with the introduction of steps. However, the trend is different in terms of trim. The original (nonstepped) Fridsma hull has the lowest trim compared to the other configurations, as shown in Figure 19(b). This finding is also reflected in the pressure resistance given in Figure 20(a), as the original Fridsma hull generates lower pressure drag. The discrepancy in results can be attributed to different hydrodynamic responses with varying planing vessel geometries, and a generalized conclusion for stepped planing hulls is not feasible.

5 Conclusions

In this study, we examined the results of CFD simulations based on RANS equations and investigated the effects of deadrise angle, chines, and transverse steps on the hydrodynamic performance of planing hulls. We first modified the original Fridsma hull form and created eight new configurations. We adopted the overset mesh method to capture the large planing hull motions and employed VOF to track the free surface using a commercial CFD code. The numerical approach was validated with the Savitsky method and the experiments available in the literature. After obtaining acceptable results in the entire Froude number range, we performed numerical simulations for the configurations and compared the results. Several conclusions derived from this study are listed below:

1) The deadrise angle substantially affects hydrodynamic performance in the planing mode. Results revealed that lower deadrise angles generate lower ship resistance at high Froude numbers. A vessel with a deadrise angle of β = 10° exhibited a 25% reduction in resistance when $Fr \geqslant 0.9$. In the displacement mode, where $Fr \leqslant 0.6$, the deadrise angle has a minimal effect on resistance, with only slight differences in trim angle and sinkage values.

2) Conf. C (planing hull with one chine) and D (planing hull with two chines) notably reduced total resistance by up to 12% and 11%, respectively. This reduction is possi-

bly due to the presence of chines, which mitigate spray patterns. In the planing regime, unlike hulls without chines, using chines shifts the center of pressure aftward, reducing the trim angle and raising the boat above the water, thus reducing wave height.

3) Unlike deadrise angle and chine numbers, stepped planing hulls did not show improvements in hydrodynamic performance. However, they increased total resistance, trim angle, and sinkage values across a wide range of Froude numbers.

In the planing regime, stepped hulls produce higher lift forces in the forebody, shifting the center of pressure forward and considerably affecting the trim angle. The absence of flow separation across all configurations prevents vortex formation behind the steps, reducing hull sinkage and wetted area. While pressure resistance dominates over friction resistance, the geometry, location, and height of the steps could enhance vortex generation, affecting total resistance. Modifications to planing vessels, such as the addition of longitudinal or transverse steps or the introduction of chines, can lead to reduced resistance, improved stability, and better seakeeping. These adjustments are expected to enhance lift, reduce bow rise, increase fuel efficiency, and achieve higher top speeds for these types of vessels. Future studies will focus on investigating these aspects further by visualizing the flow.

Nomenclature

L	Length (m)
B	Beam (m)
T	Draft (m)
D	Depth (m)
Δ	Displacement (N)
LCG	Longitudinal center of gravity (m)
l_P	Center of hydrodynamic pressure (m)
VCG	Vertical center of gravity (m)
λ	Mean wetted length-beam ratio
L_K	Keel wetted length (m)
L_C	Chine wetted length (m)
V	Speed (m/s)
β	Deadrise angle (°)
τ	Trim angle (°)
sk	Sinkage (m)
Fr	Froude number
C_V	Speed coefficient
B_{Chine}	Beam of chine (m)
C_F	Friction coefficient
R_n	Reynolds number
v	Kinematic viscosity (m^2/s)
R_P	Pressure resistance (N)
I_{YY}, I_{ZZ}	Moment of inertia ($kg \cdot m^2$)
R_F	Friction resistance (N)
R_T	Total resistance (N)
g	Gravitational acceleration (m/s^2)
ρ	Water density inertia (kg/m^3)
μ	Water dynamic viscosity (m^2/s)
u	Mean velocity in the i/j direction (m/s)
p	Average pressure (Pa)
C_{L0}	Lift coefficient at zero deadrise angle
$C_{L\beta}$	Lift coefficient at a deadrise angle
C_Δ	Load coefficient
Δt	Time step (s)
D_{Chine}	Depth of chine (m)

Acknowledgement The authors would like to acknowledge the Aero-Naval Hydrodynamics Laboratory of Marine Engineering Department, University of Sciences and Technology of Oran for its support. We also thank the staff of the Marine Robotics Laboratory at the Faculty of Naval Architecture and Ocean Engineering at Istanbul Technical University for their kind help and assistance.

Funding Supported by the UK Department for Transport, as part of the UK Shipping Office for Reducing Emissions (UK SHORE) Programme and the UK Engineering and Physical Sciences Research Council (EPSRC) [grant number EP/Y024605/1].

Competing interest The authors have no competing interests to declare that are relevant to the content of this article.

References

Begovic E, Bertorello C (2012) Resistance assessment of warped hull form. Ocean Engineering 56: 28-42. http://dx.doi.org/10.1016/j.oceaneng.2012.08.004

De Luca F, Pensa C (2017) The Naples warped hard chine hulls systematic series. Ocean Engineering 139: 205-236. http://dx.doi.org/10.1016/j.oceaneng.2017.04.038

Esfandiari A, Tavakoli S, Dashtimanesh A (2020) Comparison between the dynamic behavior of the non-stepped and double-stepped planing hulls in rough water: A numerical study. Journal of Ship Production and Design 36(1): 52-66. https://doi.org/10.5957/jspd.2020.36.1.52

Faltinsen OM (2005) Hydrodynamics of high-speed marine vehicles. Cambridge University Press. DOI: 10.1017/CBO9780511546068

Fridsma G (1969) A systematic study of the rough-water performance of planing boats. Davidson Laboratory, Stevens Institute of Technology, New Jersey, United States, Report 1275

ITTC (2011) Practical guidelines for ship CFD applications. International Towing Tank Conference. Available from https://ittc.info/media/1357/75-03-02-03.pdf [Accessed on Aug. 31, 2021]

Kahramanoğlu E, Çakıcı F, Doğrul A (2020) Numerical prediction of

the vertical responses of planing hulls in regular head waves. Journal of Marine Science and Engineering 8(6): 455. http://dx.doi.org/19.3390/jmse8060455

Lakatos M, Sahk T, Andreasson H, Tabri K (2022) The effect of spray rails, chine strips and V-shaped spray interceptors on the performance of low planing high-speed craft in calm water. Applied Ocean Research 122: 103131. https://doi.org/10.1016/j.apor.2022.103131

Matveev KI, Morabito M (2020) Hydrodynamics of planing surfaces with negative deadrise angles. Ocean Engineering 212: 107601

Menter FR, Kuntz M, Langtry R (2003) Ten years of industrial experience with the SST turbulence model. Turbulence, Heat and Mass Transfer 4(1): 625-632

Morabito MG (2014) Empirical equations for planing hull bottom pressures. Journal of Ship research 58(4): 185-200. http://dx.doi.org/10.5957/JOSR.58.4.140006

Mousaviraad SM, Wang Z, Stern F (2015) URANS studies of hydrodynamic performance and slamming loads on high-speed planing hulls in calm water and waves for deep and shallow conditions. Applied Ocean Research 51: 222-240. http://dx.doi.org/10.1016/j.apor.2015.04.007

Savitsky D (1964) Hydrodynamic design of planning hulls. Marine Technology and Sname News 1(4): 71-95

Savitsky D, DeLorme MF, Datla R (2007) Inclusion of whisker spray drag in performance prediction method for high-speed planing hulls. Marine Technology and Sname News 44(1): 35-56

Savitsky D, Morabito M (2010) Surface wave contours associated with the forebody wake of stepped planing hulls. Marine Technology and Sname news 47(1): 1-16

Stern F, Wilson RV, Coleman HW, Paterson EG (2001) Comprehensive approach to verification and validation of CFD simulations—Part 1: Methodology and procedures. J. Fluids Eng. 123(4): 793-802

Sukas OF, Kinaci OK, Cakici F, Gokce MK (2017) Hydrodynamic assessment of planing hulls using overset grids. Applied Ocean Research 65: 35-46. http://dx.doi.org/10.1016/j.apor.2017.03.015

Taunton DJ, Hudson DA, Shenoi RA (2010) Characteristics of a series of high speed hard chine planing hulls—Part 1: Performance in calm water. International Journal of Small Craft Technology 152: 55-75

Vitiello L, Mancini S, Bilandi RN, Dashtimanesh A, De Luca F, Nappo V (2022) A comprehensive stepped planing hull systematic series: Part 1 - Resistance test. Ocean Engineering 266: 112242. https://doi.org/10.1016/j.oceaneng.2022.112242

Wang H, Zhu R, Huang S, Zha L, Gu M (2023) A study on hydrodynamic characteristics of a planing hull by CFD simulation and modified MS method. Ships and Offshore Structures 18(2): 157-174. https://doi.org/10.1080/17445302.2022.2032995

Wang H, Zhu R, Zha L, Gu M (2022) Experimental and numerical investigation on the resistance characteristics of a high-speed planing catamaran in calm water. Ocean Engineering 258: 111837. https://doi.org/10.1016/j.oceaneng.2022.111837

Yousefi R, Shafaghat R, Shakeri M (2014) High-speed planing hull drag reduction using tunnels. Ocean engineering 84: 54-60. http://dx.doi.org/10.1016/j.oceaneng.2014.03.033